Journal of
Materials Chemistry A

Accepted Manuscript

This is an *Accepted Manuscript*, which has been through the RSC Publishing peer review process and has been accepted for publication.

Accepted Manuscripts are published online shortly after acceptance, which is prior to technical editing, formatting and proof reading. This free service from RSC Publishing allows authors to make their results available to the community, in citable form, before publication of the edited article. This *Accepted Manuscript* will be replaced by the edited and formatted *Advance Article* as soon as this is available.

To cite this manuscript please use its permanent Digital Object Identifier (DOI®), which is identical for all formats of publication.

More information about *Accepted Manuscripts* can be found in the **Information for Authors**.

Please note that technical editing may introduce minor changes to the text and/or graphics contained in the manuscript submitted by the author(s) which may alter content, and that the standard **Terms & Conditions** and the **ethical guidelines** that apply to the journal are still applicable. In no event shall the RSC be held responsible for any errors or omissions in these *Accepted Manuscript* manuscripts or any consequences arising from the use of any information contained in them.

Cite this: DOI: 10.1039/c0xx00000x

www.rsc.org/xxxxxx

ARTICLE TYPE

A novel route for facile synthesis of hierarchically porous TiO_2/graphitic carbon microspheres for lithium ion batteries

Chengli Zhang, Qianyu Zhang , Shifei Kang and Xi Li*

Received (in XXX, XXX) Xth XXXXXXXXX 20XX, Accepted Xth XXXXXXXXX 20XX

DOI: 10.1039/b000000x

Hierarchically porous titanium dioxide/graphitic carbon microspheres (xTiO$_2$/GCM, x = 0, 10.0, 20.0, 30.0 and 40.0) are synthesized for the first time by a simple colloidal crystal templating method. The properties of the samples are characterized by X-ray diffraction (XRD), energy dispersive spectroscopy (EDS), nitrogen adsorption–desorption (BET), scanning electron microscopy (SEM), and transmission electron microscope analysis techniques (TEM). SEM images show that all samples had similar particulate morphologies and the particle sizes are about 1 μm. And it is observed that the amount of acetone solvent had great influence on the morphology of composites. The obtained TiO_2/GCM composite microspheres possess hierarchical porosity with large specific surface area, high metallic compound content, and graphitic carbon frameworks. Employing these characteristics and advantages, the as-prepared hierarchical porous TiO_2/graphitic carbon microspheres samples are used to fabricate lithium ion battery as the active a node materials and their corresponding lithium ion insertion/extraction performance is evaluated. The resultant LIBs of the TiO_2/GCM composites possess more stable cyclic performance, larger reversible capacity, and better rate capability, compared with that of the graphitic carbon microspheres. And sample 20TiO_2/GCM exhibited a higher specific capacity, better cycling performance and rate capability than other samples.

Introduction

With the energy crisis of fossil fuels, lithium ion batteries (LIBs) are considered as the most promising energy storage technologies for electric vehicles (EVs) and renewable energy systems due to their high energy density, high voltage, and long lifespan.[1–3] However, LIBs are facing the challenges of meeting the energy and power requirements for their practical applications.[4] And new electrode materials have attracted more atteintion, which can provide higher power, longer cycle life, lower cost, and much safer.[5–13]

As the demand for alternative electrode materials for lithium ion batteries (LIBs) is rapidly increasing, TiO_2 has been regarded as a promising high-rate anode material for LIBs due to its safety, abundance in nature, chemical stability, and non-toxicity.[14,15] However, poor ionic and electronic conductivities are still the main obstacles which severely deteriorate reversible capacity and high-rate performance for their practical applications.[16–18] Carbon coating or doping may be an efficient way to resolve these problems, which are beneficial for structural stability and high-rate capability in LIBs. And carbon coated or doped have been exploited for electrode materials of LIBs.[16, 19, 20] Additionally, the special properties of hierarchically porous materials can render the enhanced electrochemical performance, which have already been reported.[21, 22] However, to the best of our knowledge, no study has been reported on the synthesis and the characteristics of hierarchically porous TiO_2/graphitic carbon microspheres used as anode materials for LIBs.

Herein, we present a novel route for facile synthesis of the hierarchically porous TiO_2/graphitic carbon microspheres (TiO_2/GCM) via colloidal crystal templating method. The synthesis was achieved using SiO_2 colloidal crystal and titanium tetrachloride as the template and Ti precursor, respectively. And the synthesized composites possess hierarchical porosity with high specific surface area and large pore volume. The as-prepared TiO_2/GCM webs as anode materials for LIBs exhibit highly effective lithium storage.

Experimental

Synthesis of composites

Colloidal SiO_2 microspheres were prepared by Stöber method[23] according to literature with 0.31 mol L^{-1} ammonia aqueous solution.

The colloidal crystal templating method was used to synthesize the hierarchically porous TiO_2/graphitic carbon microspheres. In a typical synthesis, x mmol of titanium tetrachloride (x = 0, 10.0, 20.0, 30.0 and 40.0), and 5.0 g of soybean oil were dissolved into acetone. 2.5 g of grinding SiO_2 microspheres were added to above solution and the mixture was stirred about for half hour to obtain the suspension. Then, the mixture was aged for 3 days under room temperature and transferred into a tube furnace to carbonize the precursors at the temperature of 900 ℃ under Ar

flow for 4 h with a heating rate of 2 K min^{-1}. The resultant composite was treated with 2 mol L^{-1} NaOH aqueous solution for several times to remove the silica template .

Characterization

X-ray diffraction (XRD) patterns were collected in θ-2θ mode using Rigaku D/Max2rB– Ⅱ diffractometer (CuK1 radiation, λ=1.5406Å), operated at 40 kV and 100 mA (scanning step: 5° per second). Energy dispersive spectroscopy (EDS) and scanning electron microscopy (SEM) images analysis were performed on a Philips XL-30 scanning electron microscope operating at an acceleration voltage of 25 kV. The Brumauer–Emmett–Teller (BET) method was utilized to calculate the specific surface areas. The pore size distributions were derived from the desorption branches of the isotherms using the Barrett–Joyner–Halanda (BJH) method. The total pore volume was estimated at a relative pressure of 0.99. Transmission electron microscope (TEM) images were done using a JEOL JEM-2010 electron microscope with an acceleration voltage of 200 kV.

Battery preparation

The electrochemical measurements were carried out using two-electrode coin cells (Type 2032). The sample slurry was prepared by mixing active material powders with conductive carbon (acetylene black) and polyvinylidene fluoride (PVDF) at a weight ratio of 85:10:5 in N-methyl-2-pyrrolidine (NMP). Subsequently, the slurry was coated on a copper foil using the doctor blade technique and dried at 120 ℃ for 10 h to evaporate the NMP solvent and enhance the contact between the active materials and the conductive carbons. The electrode foil was punched to 12 mm diameter discs, which were used to assemble the coin cells in an Ar glove box where both moisture and oxygen content were less than 1 ppm. Li foil was used as the counter and reference electrode in the cell. Celgard 2400 was the separator. The electrolyte solution was 1 mol L^{-1} $LiPF_6$ dissolved in a 1:1:1 mixture by volume of ethlylene carbonate (EC), dimethyl carbonate (DMC), ethylmethyl carbonate (EMC).

Electrochemical measurement

Electrochemical tests were carried out by using the above coin-type half cells. Galvanostatic charge–discharge measurements were performed on Land CT2001A (Wuhan, China) tester.

Cyclic voltammograms (CVs) was measured on an electrochemical workstation (CHI 660E) between 0.01 and 3.0 V (vs. Li/Li^+) at a scanning rate of 0.005 mV s^{-1}. Electrochemical impedance spectra (EIS) measurements were also carried out on the electrochemical workstation with a ±5 mV amplitude in the frequency range from 10 MHz to 1 MHz. All experiments were carried out at room temperature (25 ℃).

Results and discussion

Synthesis of TiO_2/GCM composites

The synthesis process of hierarchically porous TiO_2/graphitic carbon microspheres by colloidal crystal templating method[24, 25] (illustrated in Fig. 1) is actually much simpler than traditional route which involved multi-step procedures. By changing the value of *x* (the amount of TiO_2) in initial precursors, a series of hierarchically porous TiO_2/graphitic carbon microspheres composites with different TiO_2 contents are synthesized and denoted as TiO_2/GCM. Specifically, the hierarchically porous TiO_2/-graphitic carbon microspheres composite is denoted as GCM when *x* is 0.

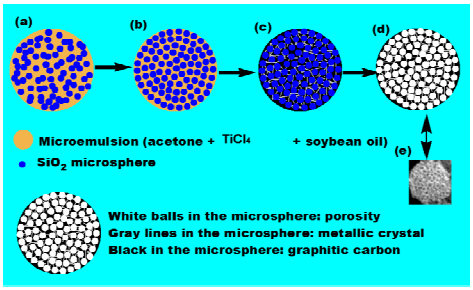

Fig.1 Illustration of the synthesis of the hierarchically porous TiO_2/graphitic carbon microspheres by colloidal crystal templating method.

Under stirring, titanium tetrachloride, soybean oil and acetone are mixed to form stable microemulsion. The microemulsion and monodisperse SiO_2 microspheres were mixed and stirred to obtain the suspension (shown in Fig. 1a). After 3 days, with the evaporation of the acetone in microemulsion droplets, the interactions between monodisperse SiO_2 microspheres increase and colloidal superparticles of SiO_2 microspheres (Fig. 1b) were formed. More specifically, the interspace between each colloidal SiO_2 microspheres is filled with microemulsion including soybean oil. The microemulsion with colloidal superparticles of SiO_2 microspheres is transferred into the tube furnace to go through the heat treatment process of carbonaceous polymerization/graphitization. Heat treatment is carried out at 900 ℃ under Ar atmosphere with a gradual increase of temperature and metallic crystal growth proceeded in situ and embedded into the graphitic carbon matrix accompanying the process of carbonaceous polymerization/graphitization (shown in Fig. 1c). The hierarchically porous TiO_2/graphitic carbon microspheres (Fig. 1d) which can be classed as colloidal superparticles[26, 27] are obtained after the silica colloidal crystal sphere templates are removed by incubating in NaOH aqueous solution under room temperature. Fig. 1e is the synthesized $10TiO_2$/GCM which is consistent with our design.

XRD analysis of TiO_2/GCM composites

Fig. 2 shows the XRD patterns of the prepared composites. XRD peaks assigned to the anatase form TiO_2 at 25° (101), 48° (200), 53° (105), 55° (211) and 63° (204) (JCPDS no. 21–1272) are seen in the as-synthesized TiO_2/GCM composites. And the peak at around 25° (002) of is overlapped by that of anatase at 25° (101) in TiO_2. Moreover, the two broad peaks of GCM sample at around 25 and 44 ° can be indexed for graphite carbon framework. With increasing content of TiO_2 in the composites, the peaks of anatase form TiO_2 become stronger, indicating the increase of size of crystals particles. The results can verify the presence of anatase form TiO_2 and graphite carbon framework in the composites, which is in good accordance with the EDX result shown in Fig. 2 (Inset is EDS spectrum of the $10TiO_2$/GCM composite). For instance, the C, Ti, and O contents of $10TiO_2$/GCM composite are 15.62 wt%, 23.99 wt%, and 60.39 wt%, respectively.

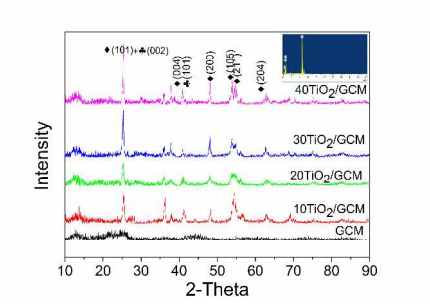

Fig. 2 The XRD patterns of GCM and TiO_2/GCM composites(Inset is EDS spectrum of the 10TiO_2/GCM composite:).

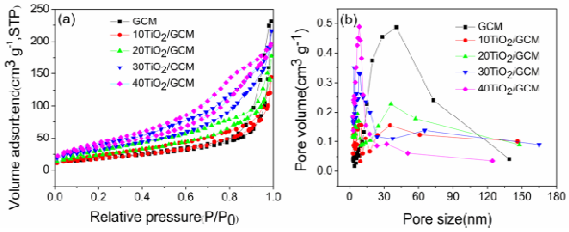

Fig. 3 (a) Nitrogen adsorption–desorption isotherms and (b) pore size distribution of the GCM and hierarchically porous TiO_2/GCM composites.

N_2 adsorption-desorption of TiO_2/GCM composites

Fig. 3 shows the nitrogen adsorption/desorption isotherms and corresponding pore size distribution curves of the porous carbons to further present their specific textural properties. As shown in Fig. 3a, all the isotherm curves show a strong uptake of N_2 as a result of capillary condensation in a wide relative pressure (P/P0) range of 0.25～0.95, which indicates the existence of multiform pore distributions.[28] Additionally, Fig. 3b reports the pore size distribution of materials. The majority of pores are located in the region of 4.36～6.42, 5.39～37.68, and 8.43～164.89 nm, which provides the evidence of hierarchical porosity of composites. The textural properties of all hierarchically porous materials are summarized in Table 1. The hierarchically porous composites generally have BET surface areas in the range of 97.97～198.75 $m^2\ g^{-1}$, total pore volumes of 0.22～0.36 $cm^3\ g^{-1}$ and the average diameter of ～5.15, ～7.87 and ～41.95 nm. It should be noted that the hierarchical porosity of composites based on the BJH method is accord with that obtained from SEM and TEM technique.

SEM and TEM analysis of TiO_2/GCM composites

The morphology of the samples is examined by means of SEM technique. Making use of 45 mL of acetone as solvent, the representative SEM images of samples are show in Fig. 4. As can be seen from the figures, the microspherical morphology of monodisperse SiO_2 template is replicated into porous materials. The original colloidal SiO_2 particles are subsequently removed, leaving behind the composites with pores that preserve the most valuable property of the colloidal crystals — the long-ranged periodic structure. The long-ranged ordering of the hierarchical porosity opens a wide variety of potential applications in areas such as optical information processing, and storage, advanced co-

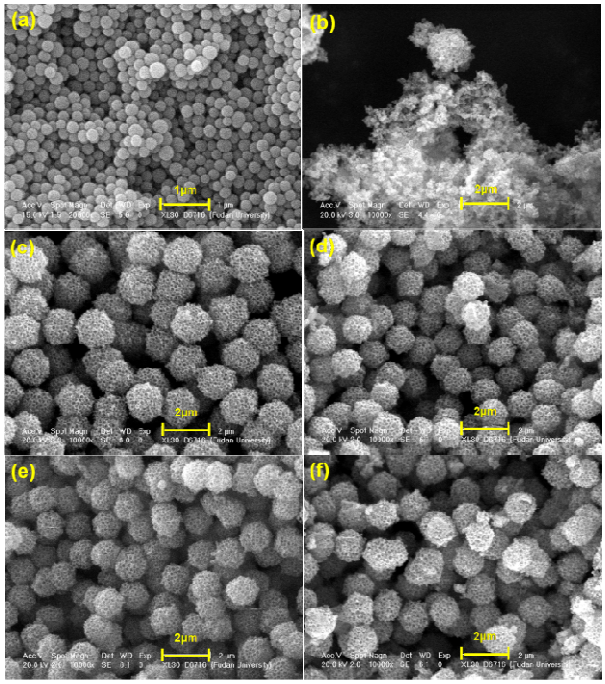

Fig. 4 SEM micrographs morphologies of SiO_2, GCM and the hierarchically porous TiO_2/graphitic carbon microspheres with the acetone amount of 45 mL: (a) SiO_2; (b) x = 0; (c) 10TiO_2/GCM; (d) 20TiO_2/GCM; (e) 30 TiO_2/GCM; (f) 40 TiO_2/GCM.

Table 1 Surface area, pore volume and pore size of the GCM and TiO_2/GCM

Samples	S_{BET} [a] ($m^2\ g^{-1}$)	V_t [b] ($cm^3\ g^{-1}$)	D_p [c] (nm)
GCM	97.967	0.17	5.11, 7.46, 40.71
10TiO_2/CM	135.90	0.27	5.88,8.28, 35.28
20TiO_2/CM	176.94	0.33	4.96, 7.14, 36.05
30TiO_2/CM	198.75	0.30	4.64, 8.12, 65.41
40TiO_2/CM	102.05	0.22	8.37, 32.28

[a] S_{BET}: the specific surface area calculated using the BET method;
[b] V_t: the total pore volume at relative pressures 0.99;
[c] D_p: the pore diameter calculated from the desorption branch of the isotherm using the BJH method.

atings and emerging nanotechnologies.[29] This valuable property are further verified by studies of N_2 adsorption test (shown in Fig. 3) and TEM images (shown in Fig. 5). The diameter of each TiO_2/GCM material is all about 1 μm, which corresponds to TEM images analysis. In particular, the structure of GCM (shown in Fig. 4b) is unstable and changed into the small pieces, which is attributed to zero TiO_2 content.

The acetone amount has great influence on the morphology of composites. While the acetone amount is changed from 45 to 15 mL, the solvent amount is not enough and the microemulsion system is not stable. With the evaporation of the acetone in microemulsion droplets, the mixture clings to bulks step by step and the obtained composites poss the conventional macroporous structure (Fig. S1).

Further evidence for the structures of these hierarchically porous TiO_2/graphitic carbon materials is provided by the TEM

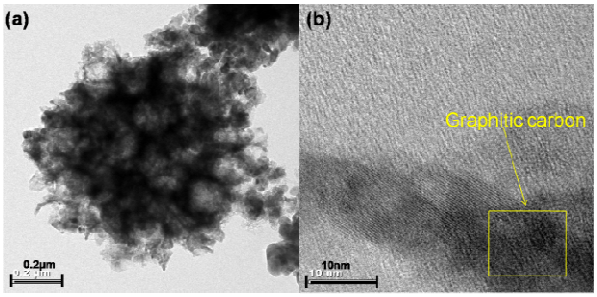

Fig. 5 TEM micrographs of 10TiO_2/GCM.

analysis. Low-magnification TEM images of 20TiO_2/GCM composites in Fig. 5 reveal that the hierarchically porous TiO_2/graphitic carbon microspheres possessing the supercrystalline structure look like the blooming lotuses, where crystals of TiO_2 are framework and carbon fills the interspace which makes microspheres more closely. The TEM images (Fig. 5) confirm that the composite has a certain degree of graphitic ordering in the framework and TiO_2 is well deposited in the hierarchically porous graphitic carbon. In additon, the analysis result of EDS, SEM and TEM technologies shows that the high metallic compound content does not destory the graphitic carbon matrix, which can widen its applicable range. All the results demonstrate that the hierarchically porous TiO_2/GCM composites have been facilely prepared via the present colloidal crystal templating method.

Lithium ion battery performance

It is well-established that the lithium ion insertion/extraction processes at anatase TiO_2 nanoparticles proceed according to the below reversible reaction: [30]

$$TiO_2 + xLi^+ + xe^- \leftrightarrow Li_xTiO_2 \quad (1)$$

The maximum value of x for a reversible reaction at room temperature is 0.5[30] and the voltage window for TiO_2-based anode materials is 1−3 V.[31] Furthermore, carbon contributes charge and discharge capacity under 1 V[32] and we set the voltage window between 0.01 to 3 V to obtain the full capacity of the composite. Fig. 6a presents the charge/discharge profiles of the TiO_2/GCM and GCM composite electrode of the 5th cycles using the CV technique at a scan rate of 0.5 mV s^{-1} between 0.01 and 3 V. All of the samples TiO_2/GCM exhibit a pair of, which can be ascribed to the Li-ion insertion/extraction in an anatase TiO_2 lattice, respectively. Additionally, the cathodic/anodic peaks of GCM at about 0.67 and 0.12 V is found to conform with Li's report.[32]

The cycling behavior was estimated at the conditions of 0.5 C charging/discharging rates as shown in Fig. 6b. It is clearly observed that doped TiO_2/GCM electrodes exhibit much higher reversible capacities than that of pristine GCM. The reversible discharge capacities are about 10TiO_2/GCM: ~ 179 mAh g^{-1}, 20TiO_2/GCM: ~ 189 mAh g^{-1}, 30TiO_2/GCM: ~ 176 mAh g^{-1}, 40TiO_2/GCM: ~144 mAh g^{-1}, respectively. After 50 cycles, the retention (10TiO_2/GCM: ~88.8 %, 20TiO_2/GCM: ~96.2 %, 30TiO_2/GCM: ~73.3 %, 40TiO_2/GCM: ~85.4 %) at 0.5 C is very high. It can be attributed to the high content of TiO_2 and the stable hierarchical structure, suggesting that TiO_2 doped is beneficial to the enhancement of the stable hierarchical structure and improvement in high-rate capability of TiO_2/GCM. And the discharge capacitiy of GCM is irreversible, decreasing from 138 mAh g^{-1}. After 10 cycles, the structure of GCM has changed and the battery can not work, which can be attributed to the zero TiO_2 content and unstable hierarchical structure.

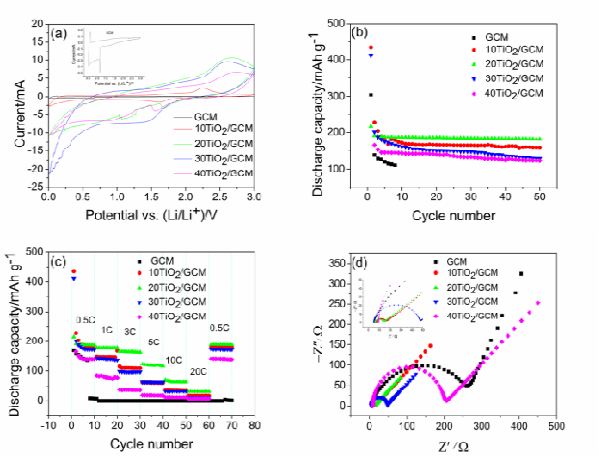

Fig. 6 Battery performance of TiO_2/GCM and GCM: (a) CVs profiles electrodes between 0.01 and 3.0 V; (b) Cycling performance at 0.5 C rates; (c) The rate capability measurements at various cycling rates; d) Electrochemical impedance spectra of the electrodes (Inset is the enlarged Nyquist plots.). All of the measurements were conducted using a voltage window of 0.01～3 V.

Fig. 6c indicates the cycling performance of the as-prepared TiO_2/GCM and GCM at different current rates of 0.5, 1, 3, 5, 10, 20 C. For each stage the charge–discharge processes of the samples are taken for 10 cycles. The cycling performance, in terms of the specific capacity, gradually declines with the increase of the current densities for all the samples. For example, at current rates of 0.5 and 5 C, the discharge capacity of 20TiO_2/GCM reduces from 191 and 123 mAh g^{-1} to 187 and 116 mAh g^{-1}, respectively. In all cases, the TiO_2/GCM composite samples exhibits better rate capability, compared with the GCM sample, which corresponds to the cycling performance (shown in Fig. 6b). Moreover, the increased pore volume should promote the capacity of as-prepared composites (in Table 1), which has been confirmed by Yu's report.[33] It may be the major reason that 20TiO_2/GCM exhibited a higher specific capacity, better cycling performance and rate capability than other samples.

The electrochemical impedance spectra (EIS) are performed for all the samples at the voltage of 1.55 V after the first cycle and the corresponding Nyquist plots are shown in Fig. 6d. And the inset is the enlarged Nyquist plots view. All the EIS curves are composed of a depressed semicircle at the high to intermediate frequency range, and there is a straight line at lowest frequency region. The high frequency semicircle is related to the charge transfer resistance at the active material interface, while the sloping line at the low frequency end indicates the Warburg impedance caused by a semi-infinite diffusion of Li^+ ion in the electrode.[34] Apparently, the TiO_2/GCM electrodes (10TiO_2/GCM:16.8 Ω, 20TiO_2/GCM:14.2 Ω, 30TiO_2/GCM: 48.1 Ω, 40TiO_2/GCM: 205.5 Ω) show a much lower resistance than the GCM electrode (260.11 Ω). The rapid diffusion of electrolyte

ions within the pores and electrons through the very thin but highly crystalline pore walls in a single porous anatase TiO_2 can contribute to the low resistance of TiO_2/GCM. Furthermore, the highly conductive graphene sheets can facilitate electron transfer from porous anatase microspheres within the whole electrode and thus decrease resistance.[35]

From the cycling performance at 0.5 C rates, rate capability measurements at various cycling rates and electrochemical impedance spectra of the electrodes, doping TiO_2 had a great degree of improvement in the capacity and the cycling performance. But with the increasing of TiO_2 doping amount, it did not always increase the positive effect of the material. Doped with 10～20%, materials had higher discharge capacity and better cycling performance in accordance to the formation of more stable structure. Doped with 20～40%, the opposite results can be obtained. So, materials doped TiO_2 could prepare as a high capacity material, and had a great rate performance in high current.

Conclusions

In summary, the hierarchically porous TiO_2/graphitic carbon microspheres were synthesized by a simple colloidal crystal templating method using SiO_2 colloidal crystal and titanium tetrachloride as the template and Ti precursor, respectively. XRD, EDS, N_2 adsorption–desorption, SEM, and TEM results all consistently reveal that the obtained TiO_2/GCM materials possess the hierarchical porosity with large specific surface area, high pore volume, and graphitic framework. Employing these characteristics and advantages, the hierarchical porous TiO_2/graphitic carbon microspheres samples exhibited much higher specific capacity ($10TiO_2$/GCM: ～ 179 mAh g^{-1}, $20TiO_2$/GCM: ～189 mAh g^{-1}, $30TiO_2$/GCM: ～176 mAh g^{-1}, $40TiO_2$/GCM:～144 mAh g^{-1}) and retention than graphitic carbon (Specific capacity :138 mAh g^{-1}). These are attributed to the rapid diffusion of electrolyte ions within the pores and electrons through the very thin but highly crystalline pore walls in the hierarchically anatase TiO_2 and facilitated electron transfer of graphitic carbon in the graphitic framework. However, the prepare of the hierarchical porous TiO_2/graphitic carbon microspheres with the more stable structure and the influence of hole sizes on the performance of lithium ion batteries still need further research and more endeavors. These works are in process.

Acknowledgements

This work was carried out with financial supports from National Natural Science Foundation of China (Grant No. 61171008), National Natural Science Foundation of China (Grant No. 21103024), Shanghai Pujiang Rencai Project (No. 09PJ1401400). This research was also supported by Dalian Mingjia Jinshu Products Limited Company, Shanghai Jubo Energy Technology Limited Company and Suzhou Baotan New Energy Limited, Company on field and fund. We would like to thank Bo Li, Shaolong Li and Wei Yuan for experimental technique support.

Notes and references

Department of Environmental Science and Engineering, Fudan University, Shanghai, China. Fax: 86-21-65642789; Tel: 86-21-65642789; E-mail: xi_li@fudan.edu.cn

† Electronic Supplementary Information (ESI) available: Fig. S1 is SEM micrographs morphologies of SiO_2 and the $10TiO_2$/graphitic carboncomposite with the acetone amount of 15 mL. See DOI: 10.1039/b000000x/

1 P. G. Balakrishnan, R. Ramesh and T. Prem Kumar, *J. Power Sources*, 2006, **155**, 401–414.
2 X. Li, X. Meng, J. Liu, D. Geng, Y. Zhang, M. N. Banis, Y. Li, J. Yang, R. Li, X. Sun, M. Cai and M. W. Verbrugge, *Adv. Functional. Mater.,* 2012, **22**, 1647–1654.
3 X. Li, A. Dhanabalan, L. Gu and C. Wang, *Adv. Energy Mater.*, 2012, **2**, 238–244.
4 D. Dambournet, I. Belharouak and K. Amine, *Chem. Mater.*, 2010, **22**, 1173–1179.
5 N. Li and C. R. Martin, *J. Electrochem. Soc.*, 2001, 148, 164-170.
6 J. Hassoun, S. Panero, G. Mulas and B. Scrosati, *J. Power Sources*, 2007, **171**, 928–931.
7 S. I. Lee, S. Yoon, C. M. Park, J. M. Lee, H. Kim, D. Im, S. G. Doo and H. J. Sohn, *Electrochim. Acta*, 2008, **54**, 364–369.
8 S. Yang, X. Feng, L. Zhi, Q. Cao, J. Maier and K. Müllen, *Adv. Mater.*, 2010, **22**, 838–842.
9 Saravanan, K.; Ananthanarayanan, K.; Balaya, P. Energy Environ. Sci., 2010, 3, 939–948.
10 T. Chen, Z. Cai, Z. Yang, L. Li, X. Sun, T. Huang, A. Yu, H. G. Kia and H. Peng, *Adv. Mater.*, 2011, **23**, 4620–4625.
11 H. Du, L. Jiao, Q. Wang, W. Peng, D. Song, Y. Wang and H. Yuan, *J. Power Sources*, 2011, **196**, 5751–5755.
12 A. Gohier, B. Laïk, K. H. Kim, J. L. Maurice and J. P. Pereira-Ramos, *Adv. Mater.*, 2012, **24**, 2592–2597.
13 X. Li and C. Wang, *J. Mater. Chem. A*, 2013, **1**, 165–182.
14 Z. Yang, D. Choi, S. Kerisit, K. M. Rosso, D. Wang, J. Zhang, G. Graff and J. Liu, *J. Power Sources*, 2009, **192**, 588–598.
15 D. Deng, M. G. Kim, J. Y. Lee and J. Cho, *Energy Environ. Sci.*, 2009, **2**, 818–838.
16 C. Lai, X. C. Yuan, X. L. Cao, Q. Q. Qiao, Y. L. Wang and S. H.Ye, *Electrochem. and Solid-State Lett.*, 2012, **15**, A65-A67.
17 X. Yang, D. Teng, B. Liu, Y. Yu and X. Yang, *Electrochem. Commun.*, 2011, **13**, 1098–1101.
18 Q. L. Wu, J. Li, R. D. Deshpande, N. Subramanian, S. E. Rankin, F. Yang and Y. T.Cheng, *J. Phys. Chem. C*, 2012, **116**, 18669−18677.
19 G. N. Zhu, Y. G. Wang and Y. Y. Xia, *Energy Environ. Sci.*, 2012, **5**, 6652–6667.
20 S. J. Park, Y. J. Kim and H. Lee, *J. Power Sources*, 2011, **196**, 5133–5137.
21 X. Wen, D. Zhang, L. Shi, T. Yan, H. Wang and J. Zhang, *J. Mater. Chem.*, 2012, **22**, 23835–23844.
22 X. Wen, D. Zhang, T. Yan, J. Zhang and L. Shi, *J. Mater. Chem. A*, 2013, **1**, 12334–12344.
23 W. Stöber, A. Fink and E. Bohn, *J. Colloid Interface Sci.*, 1968, **26**, 62–69.
24 A. Stein and R. C. Schroden, *Curr. Opin. Solid ST. M.*, 2001, **5**, 553–564.
25 X. S. Zhao, F. Su, Q. Yan, W. Guo, X. Y. Bao, L. Lv and Z. Zhou, *J. Mater. Chem.*, 2006, **16**, 637–648.
26 T. Wang, D. LaMontagne, J. Lynch, J. Zhuang and Y. C. Cao, *Chem Soc. Rev.*, 2013, **42**, 2804–2823.
27 Y. Liu, J. Goebl and Y. Yin, *Chem Soc. Rev.*, 2013, advance article.
28 Y. Wang, B. Li, C. Zhang, X. Song, H. Tao, S. Kang and X. Li, *Carbon*, 2013, **51**, 397–403.
29 O. D. Velev and A. Lenhoff, *M. Curr. Opin. IN.*, 2000, **5**, 56.
30 H. Lindstrom, S. Sodergren, A. Solbrand, H. Rensmo, J. Hjelm, A. Hagfeldt and S. E. Lindquist, *J. Phys. Chem. B*, 1997, **101**, 7717–7722.
31 D. Chen, L. Tang and J. Li, *Chem. Soc. Rev.*, 2010, **39**, 3157–3180.
32 L. H. Tang, Y. Wang, Y. M. Li, H. B. Feng, J. Lu and J. H. Li, *Adv. Funct. Mater.*, 2009, **19**, 2782–2789.
33 X. Yang, D. Teng, B. Liu, Y. Yu and X. Yang, *Electrochem. Commun.*, 2011, **13**, 1098–1101.

34 Q. Zhang, C. Zhang, B. Li, D. Jiang, S. Kang, X. Li and Y. Wang, *Electrochim. Acta*, 2013, **107**, 139–146.
35 Li, N.; Liu, G.; Zhen, C.; Li, F.; Zhang, L.; Cheng, H. M. Adv. *Funct. Mater.* **2011**, *21*, 1717.